

Article

A Simple Model for a Fast Forewarning System of Brown Tide in the Coastal Waters of Qinhuangdao in the Bohai Sea, China

Jie Wang^{1,*}, Cuiping Kuang^{1,*}, Linjian Ou², Qingchun Zhang³, Rufu Qin^{4,*}, Jiadong Fan¹
and Qingping Zou^{5,*}

¹ College of Civil Engineering, Tongji University, Shanghai 200092, China; 2011141@tongji.edu.cn (J.W.); jaydenf@tongji.edu.cn (J.F.)

² Research Center of Harmful Algae and Marine Environment, Jinan University, Guangzhou 510632, China; torangeou@jnu.edu.cn

³ CAS Key Laboratory of Marine Ecology and Environmental Sciences, Institute of Oceanology, Chinese Academy of Sciences, Qingdao 266071, China; qc Zhang@qdio.ac.cn

⁴ State Key Laboratory of Marine Geology, Tongji University, Shanghai 200092, China

⁵ The Lyell Centre for Earth and Marine Science and Technology, Institute for Infrastructure and Environment, Heriot-Watt University, Edinburgh EH14 4AS, UK

* Correspondence: cpkuang@tongji.edu.cn (C.K.); qinrufu@tongji.edu.cn (R.Q.); q.zou@hw.ac.uk (Q.Z.)

Abstract: Qinhuangdao, a famous coastal resort city in northeastern China, has been affected by the rapid growth of harmful algae. The brown tide induced by *Aureococcus anophagefferens* (*A. anophagefferens*) first occurred along Qinhuangdao's coastline in 2009, and it then developed into a harmful alga for the Bohai Sea. Based on MIKE 21, we construct a 2D coupled hydrodynamic and transport model to study the variation and distribution of total nitrogen (TN), and establish the relationship between *A. anophagefferens*, dissolved organic nitrogen (DON), and TN to provide a fast forewarning system for brown tide in Qinhuangdao. This model considers the decay, diffusion, and settling of TN, and the model results are in good agreement with the measured tidal level, current, and TN, indicating that the model is capable of capturing the observed TN distribution during the brown tide period. The transfer function relating TN to *A. anophagefferens* leads to a reliable fast forewarning and monitoring system. Moreover, the transferred *A. anophagefferens* cell density can be used to forecast the regional risk level of brown tide with a specific color indicator. The implementation of national policy relating to marine ecosystems decreases the nearshore concentration of N, P, and other nutrients, and therefore decreases harmful algal blooms. The fast routine assessment of brown tide by the present warning system provides robust guidance for the government to take action.

Keywords: brown tide; Bohai Sea; hydrodynamic and transport model; *Aureococcus anophagefferens*; forewarning system; harmful algal bloom



Citation: Wang, J.; Kuang, C.; Ou, L.; Zhang, Q.; Qin, R.; Fan, J.; Zou, Q. A Simple Model for a Fast Forewarning System of Brown Tide in the Coastal Waters of Qinhuangdao in the Bohai Sea, China. *Appl. Sci.* **2022**, *12*, 6477. <https://doi.org/10.3390/app12136477>

Academic Editor: Leonel Pereira

Received: 25 May 2022

Accepted: 24 June 2022

Published: 26 June 2022

Publisher's Note: MDPI stays neutral with regard to jurisdictional claims in published maps and institutional affiliations.



Copyright: © 2022 by the authors. Licensee MDPI, Basel, Switzerland. This article is an open access article distributed under the terms and conditions of the Creative Commons Attribution (CC BY) license (<https://creativecommons.org/licenses/by/4.0/>).

1. Introduction

Rapid industrialization and aquaculture have taken place during the past few decades in the Bohai Sea. The Bohai Sea has been one of the most important aquaculture areas in China since ancient times, producing more than 40% of the fishery resources of China. Qinhuangdao is located in Bohai Bay, a semi-closed area close to the M2 tide amphidromic point where the water is too slow to achieve self-purification [1]. Due to the high nutrient loads and organic wastewater discharges in surrounding areas and increasing sewage and industrial effluent in the aquaculture, the offshore water in Qinhuangdao is subject to frequent harmful algal blooms. Under high nutrient levels and sub-tropical temperatures, phytoplankton concentration can grow rapidly to an alarming level. Harmful tides typically last a few days to a week, depending on wind conditions, and lead to low dissolved oxygen in the bottom layer of the water [2]. Harmful algal blooms including brown tide have become more frequent, extensive, and severe worldwide [3–5].

Aureococcus anophagefferens (*A. anophagefferens*)-induced algal bloom events have received considerable attention for decades since their first occurrence in the 1980s along the eastern coast of the USA [6–8], and they were also found in the coastal bays of South Africa [9,10]. As a type of pico-sized red tide, this algal bloom has been named “brown tide” to distinguish it from traditional red tide [11], as it can discolor waters into a dark brown color. Brown tide is a discoloration of marine water due to the explosive reproduction or aggregation of planktonic algae, protozoa, or bacteria in the ocean driven by anomalous hydro-meteorological, hydrodynamic, and biological processes [12,13]. The brown tide induced by the *A. anophagefferens* in Qinhuangdao was first observed in the coastal waters near a scallop cultivation farms in 2009 [14–17], which motivated extensive investigations on the geographic and historical presence of this species in the seas of China. Tang et al. [18] investigated 3000 km of coastline and the 1500-year presence of *A. anophagefferens* and revealed that it is an indigenous species in Qinhuangdao. It took several years to confirm the causative species by microscopy, pigment chemotaxonomy, and genetic analyses [19]. Zhang et al. [12] found that all eight pelagophyte clones were similar to *A. anophagefferens*, which caused the brown tides along the coasts of the eastern United States and South Africa. Dissolved organic nitrogen (DON) and shellfish farms are mainly responsible for brown tide [20,21]. Brown tide outbreaks have become a major ecological hazard in the Bohai Sea, with significant impacts on the mariculture industry (scallops), coastal ecosystems [14,20], and zooplankton [22–27]. The main tributaries to Qinhuangdao Bay have been polluted to various degrees by industrial effluent, aquaculture wastewater, and domestic sewage. During brown tide events, peak *A. anophagefferens* concentrations were always observed along the Funing and Changli coast, where scallop cultivation farms are located in Qinhuangdao Bay.

Human activity-induced eutrophication offshore is well-recognized as the main cause of harmful algal bloom [28–30]. Lee and Qu [31] investigated algal blooms in Hong Kong and found that red tide can be formed under the right temperature, nutrient, and hydrodynamic conditions and transported to other locations. Zhang et al. [32] studied the relationship between *A. anophagefferens* distribution and environmental factors and found that certain temperature and salinity levels are required for intensive brown tide to occur in Qinhuangdao coastal water with high DON and low dissolved inorganic nutrients (DIN). Anderson et al. [28] and Glibert and Burford [33] found that eutrophication is induced by nutrient pollution close to the harmful algal area offshore. Eutrophication can impact the distribution and diversity of species and then change the preponderant algae. Wong et al. [34] proposed that algal blooms are strongly controlled by the interaction of physical and biological process. In a changing climate, an increased carbon dioxide concentration in the atmosphere is expected to intensify global warming and ocean acidification, therefore altering the distribution, frequency, and occurrence season of the red tide [35]. Brown tide events will become more frequent due to urbanization along the coast.

Previous studies into harmful algae mainly focused on species invasion or ecology deterioration. There is a lack of understanding of the formation and outbreak mechanisms of brown tide, which would be critical for establishing a reliable monitoring, forewarning, and treatment system for hot spots to prevent and reduce brown tide events. Gastrich [36] proposed a three-level hierarchy of effects of brown tide based on algal cell components. He used 35,000 and 200,000 cells/mL as concentration criteria to identify the risk level. Zhang et al. [37] used traditional modified clays to remove *A. anophagefferens* and found the removal efficiency to be low. Randhawa [38] used H₂O₂ to control brown tide in the laboratory and found that it can remove high-density *A. anophagefferens* efficiently, but the cost is high. In recent years, advanced technology has been developed to monitor harmful algae and to create a warning system. Remote sensing and satellite observations have been applied to track the spatial distribution and growth of algae. Numerical models have been applied to provide harmful algal warnings [39,40]. Using physical and chemical methods to treat brown tide and other harmful algal bloom events, however, is still in its infancy.

In this study, a coupled hydrodynamic and particulate transport model based on MIKE21 is employed to predict the temporal and spatial distribution of the total nitrogen (TN). This model considers the decay, diffusion, and settling of TN, and the model results are in a good agreement with the measured tidal level, current, and TN, which indicates that the model is capable of capturing the observed TN distribution during the brown tide period. A relationship between *A. anophagefferens*, dissolved organic nitrogen (DON), and TN is obtained from field observations and combined with numerical simulation results of TN to establish a fast forewarning system for brown tide in Qinhuangdao. The objective is to make full use of the observation data to establish a reliable relationship between *A. anophagefferens* and TN to represent the complex process of algal growth in order to provide fast alerts for the stakeholder. The main simulated area in this study is shown in Figure 1.

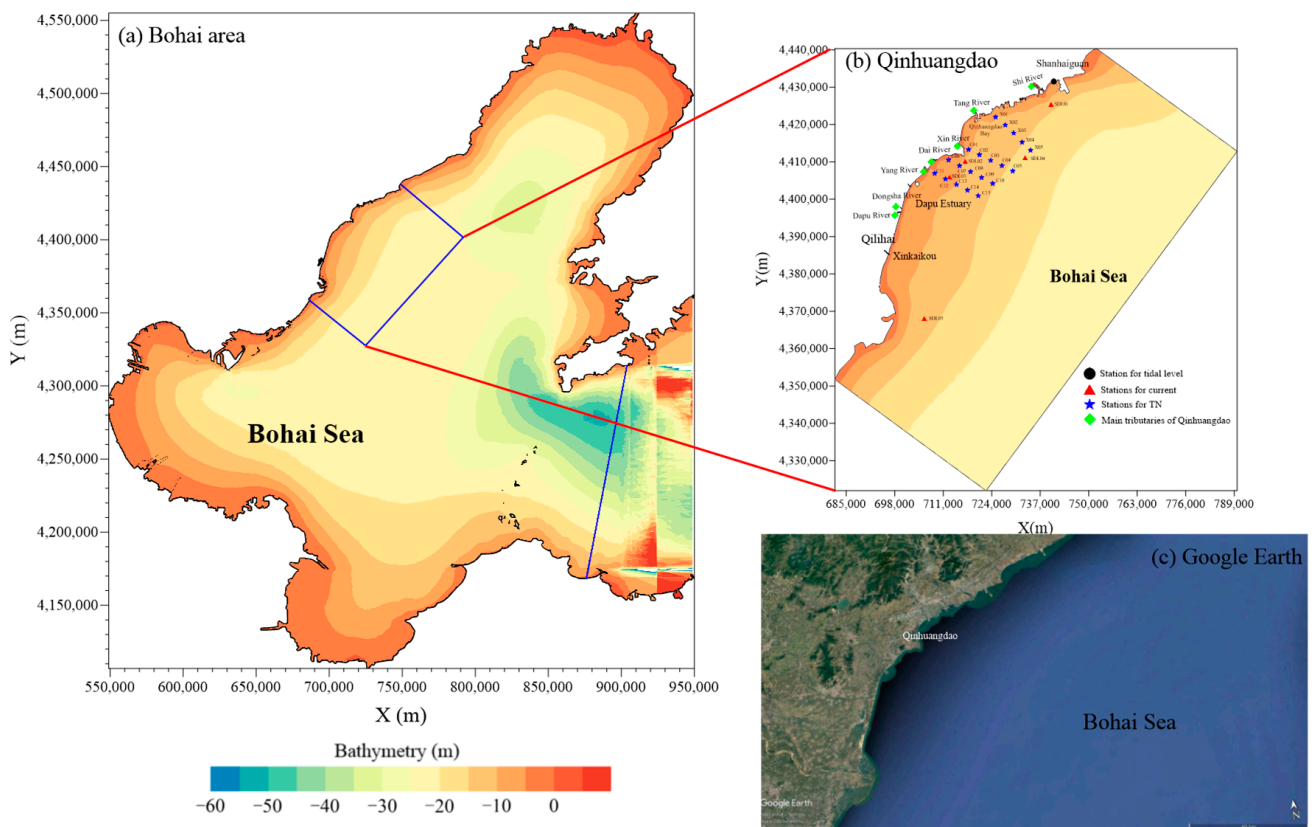


Figure 1. (a) The Bohai Sea area; (b) the main study area and the field observation stations (the black circle represents the tidal level station, the red triangles are the current stations, and the blue pentagrams show the position of TN stations). (c) Google Earth view of Qinhuangdao and the Bohai Sea.

2. Materials and Methods

MIKE 21 was developed by the DHI Group and can continuously simulate tidal circulation and mass transport. In this study, we established a two-dimensional coupled hydrodynamic and mass transport model of Qinhuangdao using a flow model (FM) based on the flexible unstructured mesh method, which was developed for applications within oceanographic, coastal, and estuarine environments. The spatial discretization of the primitive equations was performed using an element-centered finite volume method. The spatial domain was discretized by the subdivision of the continuum into non-overlapping elements. The MIKE FM has been used in many studies, and the governing equations and details of this model can be found in the MIKE User Manual [41].

2.1. Study Area and Mesh

Brown tides commonly occur in summer, especially in July and August, along the Qinhuangdao coastline. This model included two parts with different scales. A double-level scheme of unstructured triangular meshes with different refinements and scales was set up as shown in Figure 2. The large mesh (Level 1) covered the whole Bohai Sea to ensure a correct tidal flow field, and it provided the water level and current boundary to the small mesh (Level 2). The small mesh covered Qinhuangdao coastal waters, including the main river outlets. The Bohai Sea model was driven by the time series of the tidal level at Dalian and Yantai (two ends of the open boundary in Figure 2) from the tidal table published by the National Marine Data and Information Service of China. The Qinhuangdao model was driven by the time series of the water level, current speed, and direction extracted from the computational results of the Bohai Sea model along three open boundaries. The boundary of the small mesh was from the Luan River to the Shi River Estuary, along the coastline with a length of 16.5 km in the northeast and 35.6 km in the southeast. The large and small meshes had 14,183 and 13,606 nodes with 23,419 and 25,301 elements, respectively. The mesh size generally decreased from the sea toward the coast and estuary when considering both computational time and accuracy.

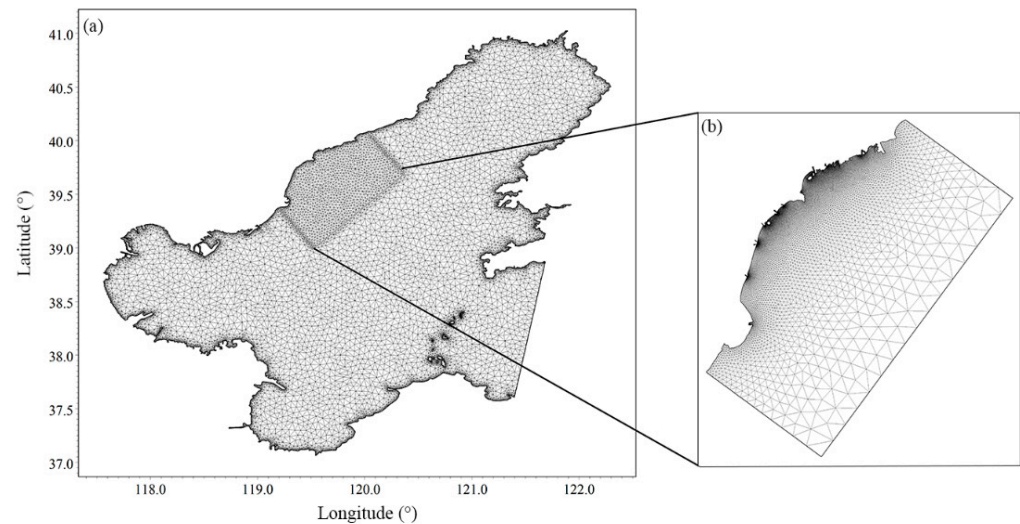


Figure 2. The nested model domain and mesh. (a) The regional model domain and mesh of the Bohai Sea; (b) The local model domain and mesh of Qinhuangdao.

2.2. Hydrodynamic Model

The transport model was based on the currents calculated by a hydrodynamic model. Given that the coverage area of brown tides is restricted to the shallow intertidal and subtidal zones, a 2DH model mesh was adequate to simulate the hydrodynamics of the study area, considering the balance of computational speed and model precision in Qinhuangdao [42,43]. The model solved the two-dimensional incompressible Reynolds-averaged Navier–Stokes equations with assumptions of Boussinesq and hydrostatic pressure. The computational mesh used in this research was unstructured triangular mesh with the spatial discretization adopting the cell-centered finite volume method. The continuity and momentum equations were converted into nonlinear shallow water equations by integrating them over depth, and the 2DH equations are shown as follows:

$$\frac{\partial h}{\partial t} + \frac{\partial hu}{\partial x} + \frac{\partial hv}{\partial y} = hS \quad (1)$$

$$\frac{\partial hu}{\partial t} + \frac{\partial hu^2}{\partial x} + \frac{\partial huv}{\partial y} = fvh - gh \frac{\partial \eta}{\partial x} - \frac{h}{\rho_0} \frac{\partial p_a}{\partial x} - \frac{gh^2}{2\rho_0} \frac{\partial \rho}{\partial x} + \frac{\tau_{sx}}{\rho_0} - \frac{\tau_{bx}}{\rho_0} - F_u + hu_s S \quad (2)$$

$$\frac{\partial hv}{\partial t} + \frac{\partial huv}{\partial x} + \frac{\partial hv^2}{\partial y} = -fuh - gh \frac{\partial \eta}{\partial y} - \frac{h}{\rho_0} \frac{\partial p_a}{\partial y} - \frac{gh^2}{2\rho_0} \frac{\partial \rho}{\partial y} + \frac{\tau_{sy}}{\rho_0} - \frac{\tau_{by}}{\rho_0} - F_v + hv_s S \quad (3)$$

where t is the time; x and y are the Cartesian coordinates; u and v are the depth-averaged velocity components in the x and y directions; h is the sum of the still water depth, d , and the time-varying water level, η ; S is the discharge of the point sources; f is the Coriolis parameter related to the angular velocity of Earth's rotation and the geographic latitude; g is the gravitational acceleration; ρ is the water density; ρ_0 is the reference water density; P_a is the atmospheric pressure; τ_{sx} and τ_{sy} are the surface stresses induced by wind; τ_{bx} and τ_{by} are the bottom stresses; F_u and F_v are the horizontal stress terms due to eddy viscosity; and u_s as well as v_s are the discharge velocities of the point sources.

The model adopted wet-dry dynamic boundary processing technology, and the critical water depths of dry and wet points were 0.005 m and 0.05 m, respectively. The computational time step was in the range of 0.1–30 s and was adjusted to meet the Courant–Friedrich–Lewy (CFL) condition with a limited value of 0.8 in the model calculation process, where $CFL = (\sqrt{gh} + |u|) \frac{\Delta t}{\Delta x} + (\sqrt{gh} + |v|) \frac{\Delta t}{\Delta y}$. The horizontal eddy viscosity coefficient used the Samagorinsky model to calculate the grid scale, and the Samagorinsky coefficient was 0.28. The initial velocity and water level were 0 m/s and 0 m, respectively. The Manning number was 74 m^{1/3}/s, by which the model bed resistance was determined. Based on the Bohai Sea model, the boundary condition at the tidal inlet and open sea boundaries was adopted for the medium tidal range and Flather condition, respectively [42]. The boundary condition at the river outlet was set as the specified discharge value of 1 m³/s, and the initial condition was set as 0, including values of surface elevation, u-velocity, and v-velocity. The time step interval could self-regulate itself, ranging from 0.01 to 30 s to meet the CFL restriction as velocity changed with time at all computational nodes and time steps. The wind and temperature data were downloaded from the European Centre for Medium-Range Weather Forecasts (ECMWF (<http://apps.ecmwf.int/datasets/data/interim-full-daily>, accessed on 1 January 2021)) with a spatial resolution of 0.25°.

2.3. Transport Model

We set the TN as a component of the transport model. There was no dispersion across open boundaries, as the gradient of the concentration here was assumed to be 0. The linear decay of a component is generally defined as:

$$\frac{\partial c}{\partial t} = -kc \quad (4)$$

where c is the specific concentration and k is the decay constant.

For simulating the variation of TN distribution, after conducting many tests, we set the parameter of decay as 1.157×10^{-7} /s. The time step was the same as that of the hydrodynamic simulation. The initial component of TN was set as 5 mg/L according to the measured data. The discharge and TN components of the main rivers were based on the field-measured data collected.

2.4. Model Validation

Field observations of tidal level and current were used to verify the hydrodynamic model. The water levels were collected from the Shanhaiguan station during the spring tide (11–12 May 2013) and neap tide (16–17 May 2013). The current data were collected at five field stations, SDL01 to SDL05, during the neap tide, 16–17 May 2013. These observation stations are shown in Figure 1. Figure 3 shows the comparison of simulated results and measured data including tidal level and current speed and direction. The hydrodynamic model results were quantitatively assessed against observed values using the *skill* model [44].

$$skill = 1 - \frac{\sum |X_m - X_o|^2}{\sum (|X_m - \bar{X}_o| + |X_o - \bar{X}_o|)^2} \quad (5)$$

where \bar{D} is the mean value, in situ, of the observed data; M and D are the computed result and in situ observed data, respectively; and N is the number of data entries. A *skill* value of 1.0 indicates a perfect performance of the model: *skill* between 0.65 and 1 is considered excellent, *skill* in the range of 0.5–0.65 is considered very good, *skill* in the range of 0.2–0.5 is considered good, and *skill* of less than 0.2 is considered poor.

The model results generally matched the measured values very well with the excellent performance of *skill* evaluation summarized in Table 1. The *skill* of tidal level at Shanhaiguan during the spring and neap tides were all 0.99, and those of current speed at SDL01, SDL02, SDL03, SDL04, and SDL05 were 0.90, 0.87, 0.85, 0.94, and 0.86, respectively. The *skill* values of current direction at the same stations were 0.97, 0.98, 0.95, 0.97, and 0.95, respectively. All *skill* values (over 0.90) were much larger than 0.65, implying the excellent predictive efficiency of the model.

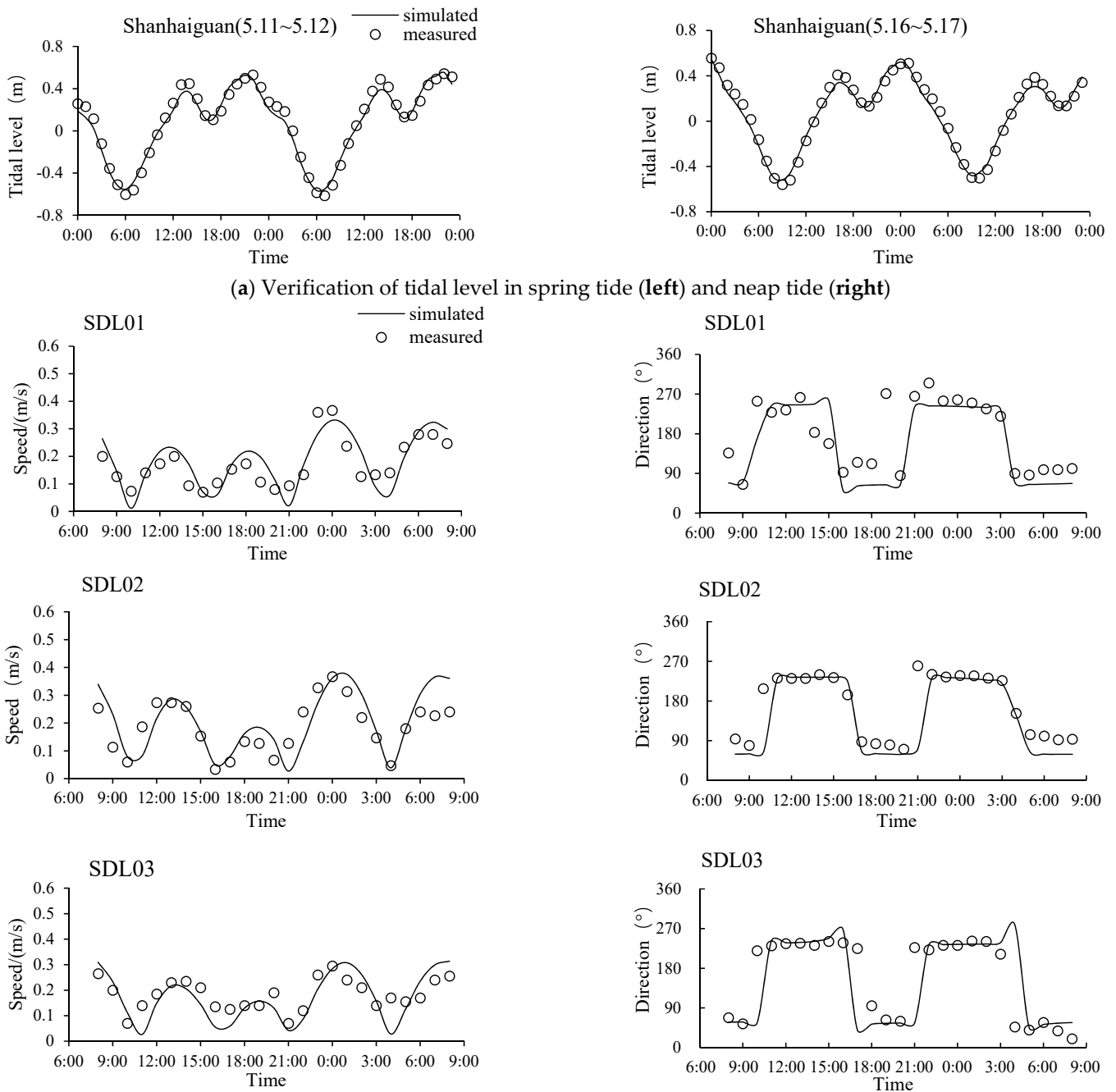
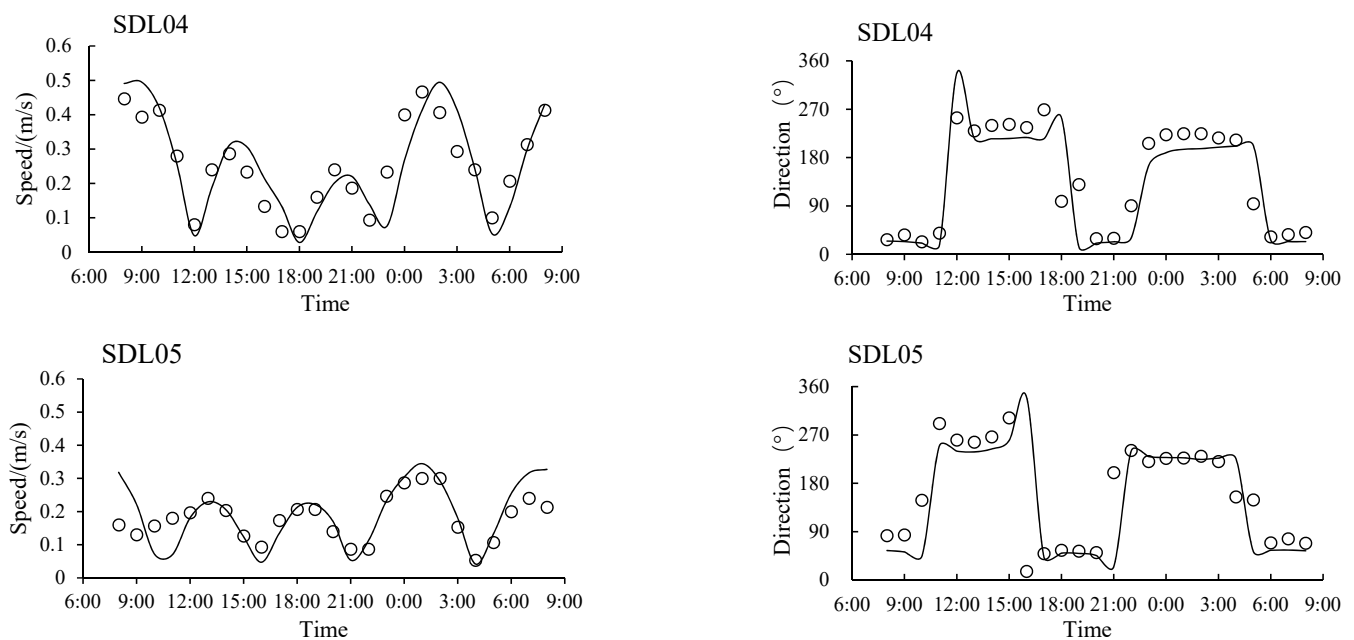


Figure 3. Cont.



(b) Verification of current speed and direction at five current stations

Figure 3. Model validation of tidal level and current velocity.**Table 1.** Hydrodynamic model evaluation.

Variable	Time	Station	Period	Skill	Performance
tidal level	May, 2013	Shanhaiguan	Neap tide	0.99	excellent
		Station	Spring tide	0.99	excellent
speed	May, 2013	SDL01		0.90	excellent
		SDL02		0.87	excellent
		SDL03	Neap tide	0.85	excellent
		SDL04		0.94	excellent
		SDL05		0.86	excellent
direction	May, 2013	SDL01		0.97	excellent
		SDL02		0.98	excellent
		SDL03	Neap tide	0.95	excellent
		SDL04		0.97	excellent
		SDL05		0.95	excellent

In order to evaluate the transport model, which shares the same computational mesh as the hydrodynamic model of Qinhuangdao, the validated TN concentration data were collected from Qinhuangdao during the period 16–23 July 2013. The simulated result of TN concentration is shown in Figure 4. Given that the measured data at 20 stations were from different dates, the time series was discontinuous, we calculated the average error, and all of the numbers were below 11% (shown in Table 2), which means the present model can accurately predict the TN distribution.

Table 2. The average error of TN for July 16–18 2013.

Time	Average Error of Station Groups (%)	
	X Group	C Group
16 July 2013	4.05	2.40
18 July 2013	3.73	8.60
23 July 2013	6.64	8.81
25 July 2013	10.45	10.45
Average	6.22	7.57

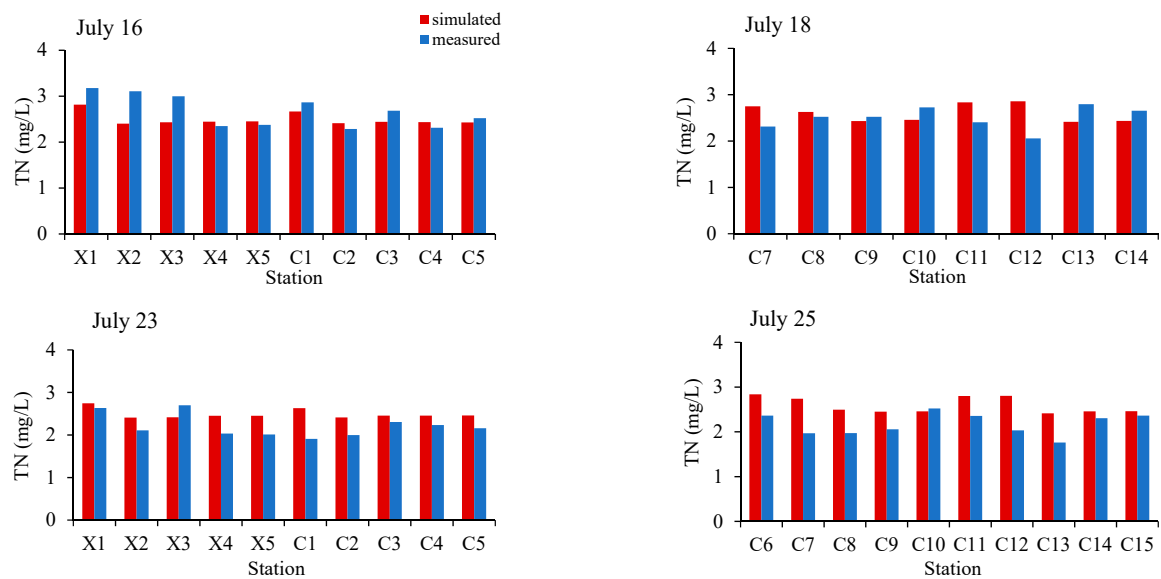


Figure 4. Verification of the TN concentration.

3. Results

In this section, we firstly use the coupled hydrodynamic and transport validated model to simulate the TN concentration during the brown tide period in 2014. The TN concentration in the coastal water is mainly controlled by the seagoing rivers. We then find the relationship between the TN concentration and *A. anophagefferens* density by studying the observed data at 20 stations and transfer the TN to DIN, and then to *A. anophagefferens*. Furthermore, we establish an indicator system with four grades and provide appropriate measures for application.

3.1. TN Distribution during Brown Tide

Figure 5 shows the measured and simulated data of TN concentration at 20 stations. The simulation period is from March to September 2014 and includes two large-scale brown tide events in May and August, respectively. As we lack the seagoing rivers' TN input data for 2014, considering that there are no large construction projects and the climate only changed slightly, we use the data for 2013 to take the place of the data for 2014. We can see that the result shows a certain deviation, which may be mainly caused by the difference in TN concentration from 2013 to 2014 in the seagoing rivers. Although there is this weakness, the simulation deviation is controlled at 26%, indicating that the results are reasonably convincing. Figure 6a presents the distribution of TN during the brown tide period in 2014, and Figure 6b depicts the satellite-observed bloom-area for the same period. We can see that these two figures are similar to each other in the abnormal area, although the simulated one covers more area, which demonstrates that the TN is correlated with brown tide. It is shown that, in the coastal area, the TN concentration is higher than that of the open sea, indicating that there is a higher risk along the coastline of having an algal bloom event.

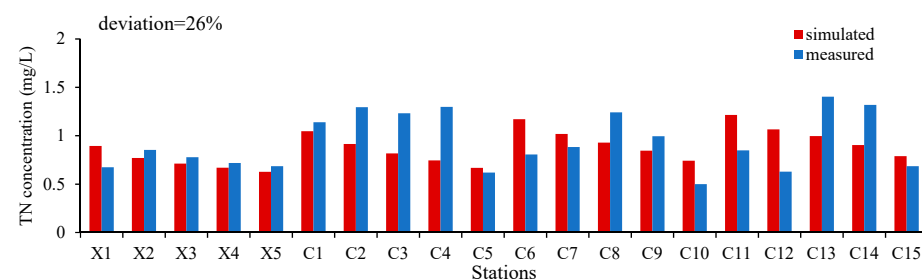


Figure 5. The simulated results compared with measured data at selected stations in May 2014.

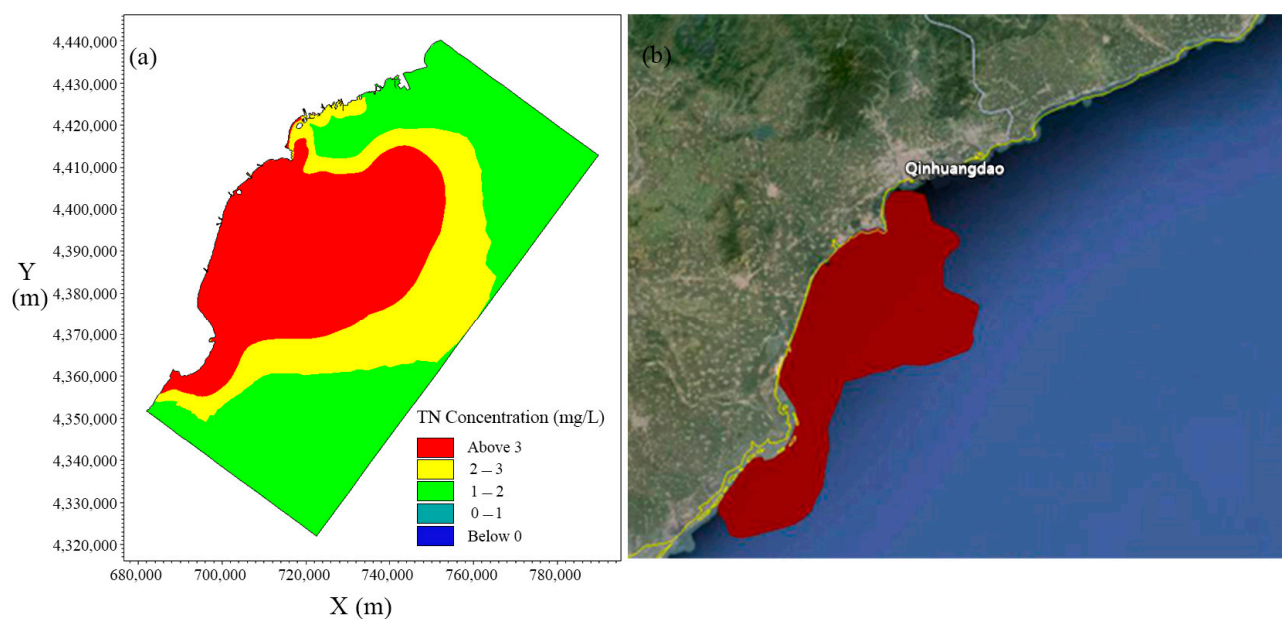


Figure 6. (a) The distribution of TN concentration during the brown tide period in May 2014. (b) The satellite-observed brown tide area in May 2014.

3.2. Transfer Function from TN to *A. anophagefferens*

A. anophagefferens is a tiny, spherical and nonmotile picoplanktonic (cell size 2–3 μm) pelagophyte with no flagella [18,45]. *A. anophagefferens* cells were abundant during the brown tide period in Qinhuangdao coastal waters, which can be seen as an indicator of brown tide. Zhang et al. [32] reported that *A. anophagefferens* abundance was strongly positively correlated with nitrite and temperature. DON is commonly thought of as the main nitrite resource, and it is vital for improving *A. anophagefferens*-induced brown tide [46,47]. Since nitrogen is routinely monitored as a chemical element discharged from rivers to sea along the coastline in Qinhuangdao, we seek the relationship between *A. anophagefferens* density and TN concentration through their correlations with DON.

We analyzed the measured data from June 2013 to August 2014, which included two large-scale brown tide events (May 2013 and August 2014) in the sea area. The observation data indicates strong correlation between *A. anophagefferens* cell density and DON and temperature (T). Figure 7 shows the relationship between the *A. anophagefferens* density (use the cells concentration to represent) and DON in 2013 and 2014 during the brown tide event periods. Commonly, a concentration of 5×10^7 cells/L is thought of as the warning indication value to represent brown tide, and we use red circles to mark these values in this figure. As shown in Figure 7a, the density of *A. anophagefferens* cells increases when the concentration of DON is in the range of 0.00~40.00 $\mu\text{mol/L}$ and the value reaches a relatively high grade. Therefore, we narrow the range of DON concentration to 10.00~30.00 $\mu\text{mol/L}$ and find that the density of *A. anophagefferens* distributes in every value, which implies that the DON concentration is not the only main factor that influences the *A. anophagefferens* cell density in this range. When the range continuously narrows to 30.00~40.00 $\mu\text{mol/L}$, the measured data reduce but the density of *A. anophagefferens* cells significantly increases, showing that the DON concentration varies in this range and it becomes the main factor of *A. anophagefferens* cell growth. In Figure 7b, the data in 2014 are similar to the data collected in 2013, showing that the *A. anophagefferens* cells rapidly grow in the range of 30.00~40.00 $\mu\text{mol/L}$, and the concentration is higher than the indicated value. As can be seen in the range of 50.00~60.00 $\mu\text{mol/L}$, there is also a point above the warning indication concentration, which means the brown tide can still bloom. However, if the DON concentration is lower than 20.00 $\mu\text{mol/L}$, the possibility of bloom becomes lower, indicating that a low concentration can inhibit the propagation of *A. anophagefferens*. Combined with Figure 6a, although the data for DON are finite, the

range of DON concentration from approximately 20.00 to 60.00 $\mu\text{mol/L}$ can be seen as the sensitive range for inducing brown tide. With the DON concentration increase, a higher *A. anophagefferens* cell density can cause the brown tide event with more certainty.

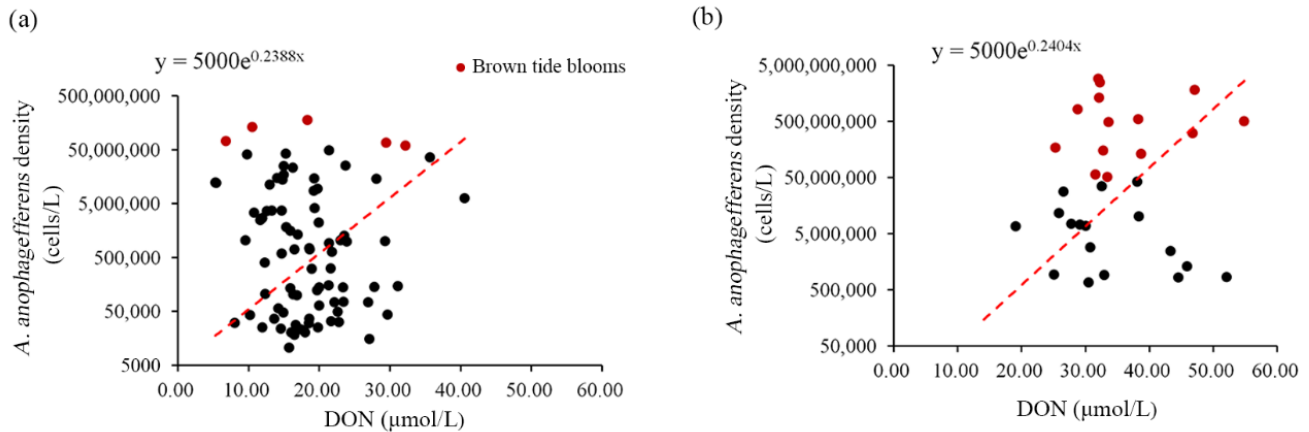


Figure 7. The relationship between *A. anophagefferens* cell density and DON in 2013 (a) and 2014 (b).

Separately drawing the fitting relationship in Figure 7a,b, we can see that, in Figure 7b, the data are substantial and the time covers four months, providing greater accuracy than in Figure 7a. So, we preliminarily choose the fitting equation of the data in 2014 to establish the relationship of *A. anophagefferens* cell density and DON concentration as an exponential function:

$$\rho = 5000e^{0.24DON} \tag{6}$$

where ρ is the *A. anophagefferens* cell density.

In this study, temperature is not the main factor affecting the transformation, but for rigor and accuracy, we still clarify it in this section and set the most appropriate value in the numerical model. We also draw a relationship between the temperature (T) and *A. anophagefferens* cell density in Figure 8. *A. anophagefferens* concentration reaching the warning indication level in the range of 10~23 $^{\circ}\text{C}$ is rare; however, in the range of 23~28 $^{\circ}\text{C}$, the concentration rapidly increases. From Figure 8, we can obviously see that the most appropriate temperature for *A. anophagefferens* growth is around 23~26 $^{\circ}\text{C}$, which is slightly higher than the study that gave the appropriate temperature as ranging from 21.5 to 23.2 $^{\circ}\text{C}$ [32].

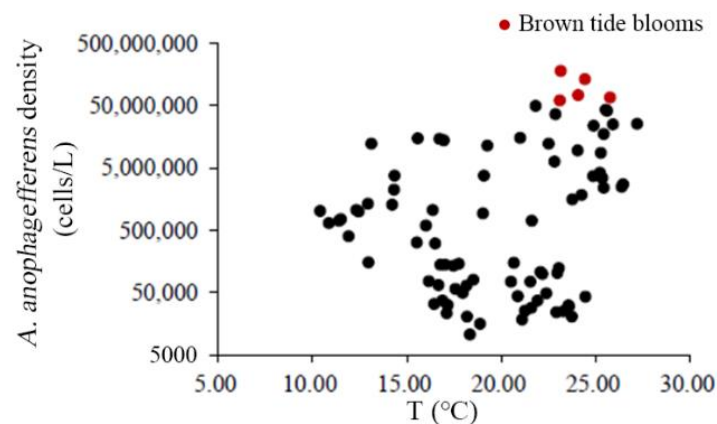


Figure 8. The relationship between T and *A. anophagefferens* density from June to July in 2013.

Based on the correlation between the *A. anophagefferens* cell density and DON concentration during the brown tide periods, we tried to explore the correlation between *A. anophagefferens* cell density and TN concentration in the long-term measured data. There are

no sufficient data, so we used the existing data to analyze the correlations of TN–DIN and DIN–DON and then transferred the relationship to TN concentration–*A. anophagefferens* cell density to obtain the mechanism of TN concentration’s effect on *A. anophagefferens* growth.

Figure 9 shows the relationship between the measured concentration of DIN and TN at 20 stations (time series are from June to July in 2013 and from April to August in 2014; positions are shown in Figure 1b). The intercepts are all set as 0, because the DIN and DON are also 0 mg/L when the TN concentration is 0 mg/L. All determination coefficients (R^2) are above 0.53, indicating that the fitting relationships are reasonable. The slope of every station is summarized in Table 3, and the average value is 0.195.

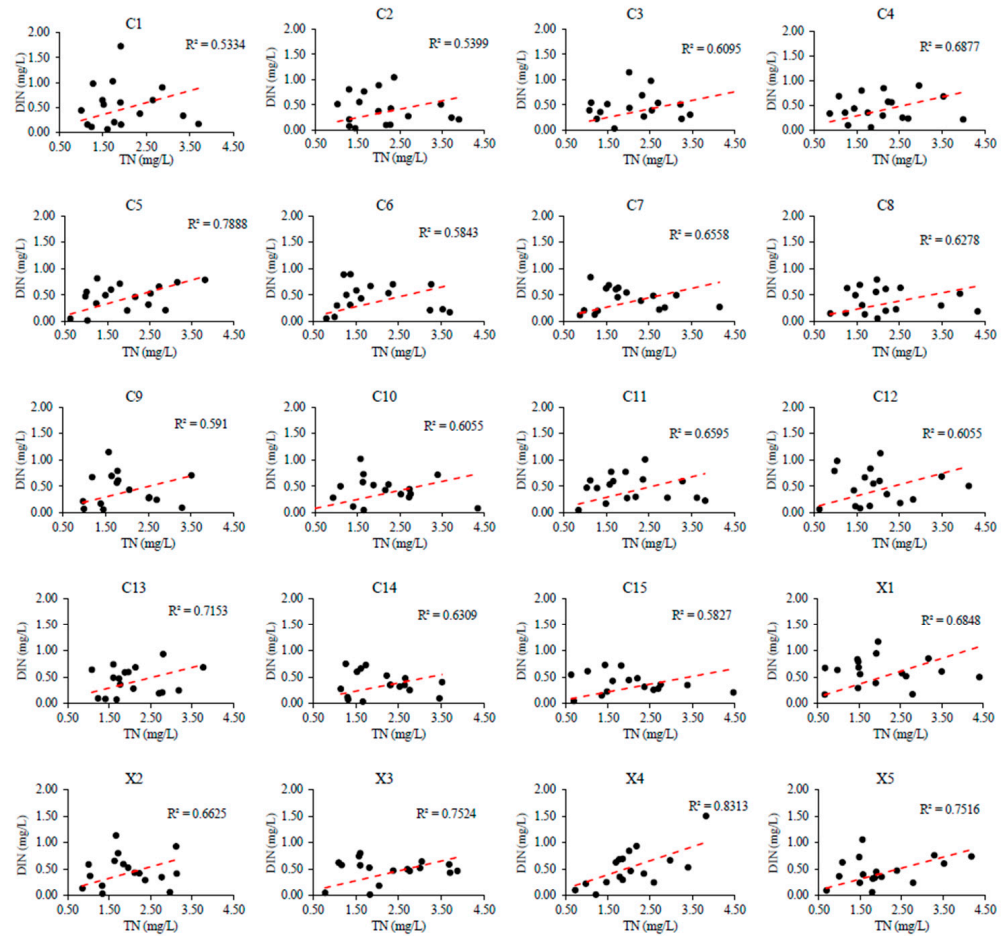


Figure 9. The relationships between DIN and TN at 20 stations from June 2013 to August 2014 derived from the field observations at station X1 to X5 and C1 to C15.

Table 3. The slope of fitted linear relationship between DIN and TN at 20 stations from June 2013 to August 2014.

Stations	DIN/TN	Stations	DIN/TN	Stations	DIN/TN	Stations	DIN/TN
C1	0.239	C6	0.186	C11	0.195	X1	0.243
C2	0.166	C7	0.179	C12	0.214	X2	0.217
C3	0.169	C8	0.155	C13	0.198	X3	0.186
C4	0.193	C9	0.200	C14	0.155	X4	0.263
C5	0.224	C10	0.170	C15	0.146	X5	0.208
Average value				0.195			

Based on the measured data of TDN, DIN, and DON, we also draw the fitting curves of DIN–TDN and DON–TDN and calculate R^2 using the same methods. All determination coefficients (R^2) shown in Figure 10 are above 0.82, indicating that the fitting relationships

are good. The average slope values of DIN–TDN and DON–TDN, as shown in Table 4, are 0.450 and 0.550, respectively. Furthermore, we transferred these two groups of relationship to establish that the slope of DON–DIN is 1.222. Combined with the slope of DIN–TN, we finally obtain that the averaged DON/TN is 0.238.

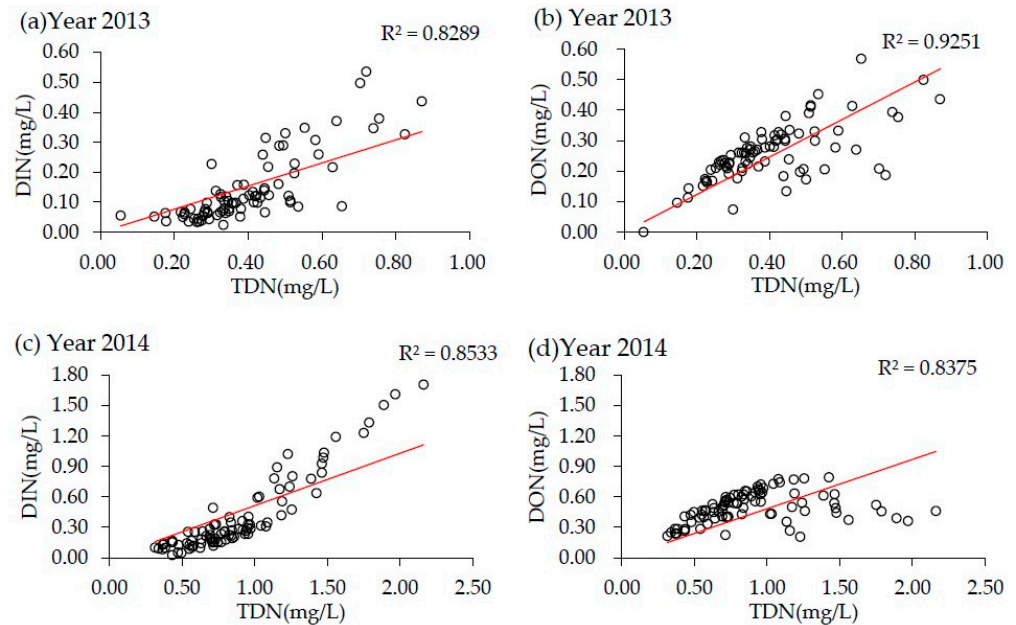


Figure 10. The relationships of DIN–TDN and DON–TDN at 20 stations from June 2013 to August 2014.

Table 4. Summary of the values of DIN/TDN and DON/TDN.

Period	DIN/TDN	DON/TDN
June to July 2013	0.385	0.615
April to August 2014	0.515	0.485
Average	0.450	0.550

Based on the correlation of DON–TN and DON–*A. anophagefferens* cells, we derived the fitting equation of *A. anophagefferens* cell density and TN concentration as below:

$$\rho = 5000e^{4.087TN} \tag{7}$$

3.3. Fast Forewarning System of Brown Tide

The brown tide in the coastal area of Qinhuangdao was induced by DON and shellfish aquaculture [16,20] and, conversely, the brown tide also influences the shellfish. The brown tide in 2009 resulted in shellfish death in two out of three of the mariculture areas in Qinhuangdao. Meanwhile, the brown tide event in 2010 covered more than 3350 km², which caused the pecuniary loss of more than 0.2 billion RMB [48]. We indirectly transferred the DON concentration to the *A. anophagefferens* cell density using the TN concentration as mentioned before.

According to the current situation, we separated the system into four grades in Table 5 to help the government to take appropriate measures to prevent brown tide from occurring or spreading. This system setup uses the relationship between TN and *A. anophagefferens* density on the basis of the transport model results to compartmentalize grades. Green represents good water quality, and the government should only conduct routine monitoring; meanwhile, when the water quality worsens and brown tide occurs, it needs to take appropriate measures.

Table 5. The brown tide warning and fast forecast monitoring indicator of *A. anophagefferens* density.

<i>A. anophagefferens</i> Density (Cells/L)	Grade	Represent Color	Measures
$< 5 \times 10^5$	Safe	Green	Conduct routine monitoring
$5 \times 10^5 \sim 5 \times 10^6$	Third-degree	Yellow	Conduct Third-degree forecast
$5 \times 10^6 \sim 5 \times 10^7$	Second-degree	Orange	Warning for shellfish aquaculture
$> 5 \times 10^7$	First-degree	Red	Brown tides—Conduct emergency handling for shellfish aquaculture

Meanwhile, we have highlighted the transferred *A. anophagefferens* distribution in August 2014 with the appropriate color in Figure 11. It is clear that *A. anophagefferens* density in this period for most of the area offshore is in the range of approximately 5×10^5 to 5×10^6 cell/L, in the system shown as the third degree. However, there is also a small area in the range of $5 \times 10^6 \sim 5 \times 10^7$ cell/L close to the seagoing rivers, which is indicated as second degree, meaning that the government needs to take relevant measures to address this higher concentration.

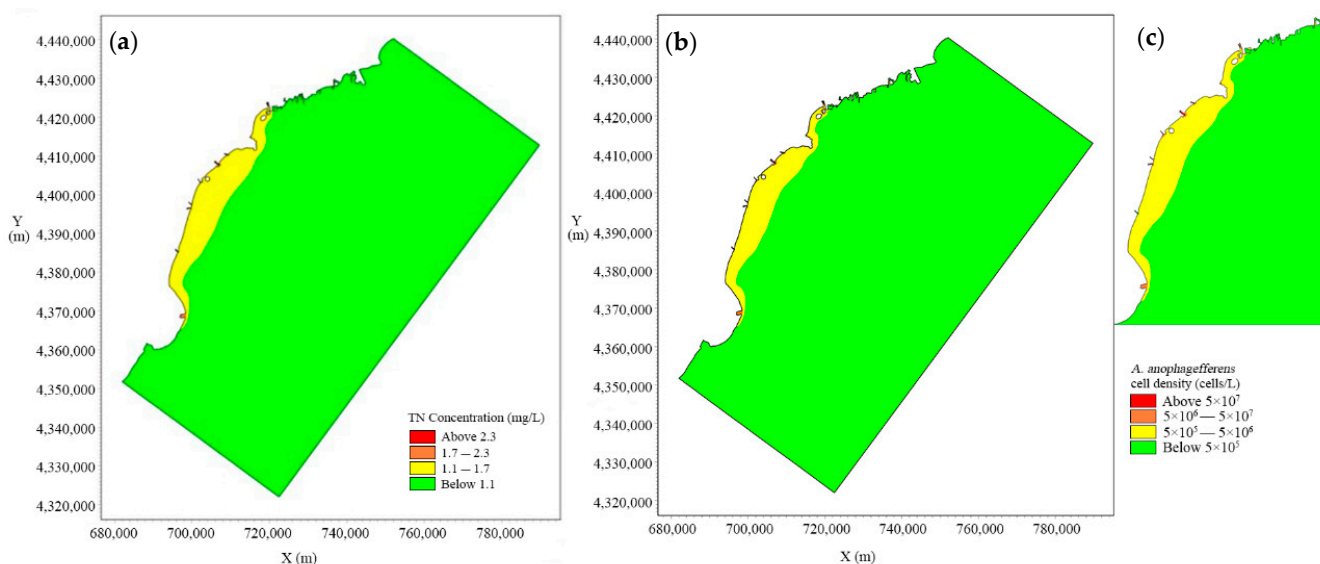


Figure 11. (a) The distribution of TN concentration in August 2014; (b) the transformation results from TN concentration to *A. anophagefferens* cell density, and amplification of the bloom area (c).

Although this forewarning system uses a simple mechanism and model, it still provides a fast prediction for brown tide outbreaks and helps to carry out total management in the mariculture areas. The system uses routine monitoring data as the input, which is convenient for operation. Meanwhile, the result indicator provides different degrees of warning for the government to quickly conduct monitoring in the key areas of potential risk and take appropriate actions in mitigating brown tide.

4. Discussion

4.1. Impact of Nutrients on Brown Tide

During the Thirteenth Five-Year-Plan period, the Science and Technology Ministry of China conducted special studies on typical harmful algal blooms in offshore areas. In 2017, a project examining the formation mechanism, monitoring, and forecasting and estimate technology of red tide (include brown tide) started. Aiming at algal bloom in offshore areas, many scholars have conducted studies into monitoring and water environmental treatment. Using modified clays is an important technique for the mitigation of harmful algal blooms, especially the red tide [49], and has been successfully applied in offshore red tide management in China, greatly improving coastal water quality. Hebei province has promulgated the plan for comprehensive control in the Bohai Sea and advocated improving

the marine environmental risk monitoring and forecasting and emergency management capability. Policy demands that in the ecologically fragile region and the brown tide-prone area, the feeding aquaculture model is forbidden. Meanwhile, carrying out the risk assessment of emergencies in coastal cities to improve the ability of the government to prevent environment risk events is also a vital measure. All of these measures have great effects on reducing harmful algal bloom. Figure 12 shows the occurrence number of red tide (include brown tide) and the coverage of *A. anophagefferens* from 1990 to 2020 (data collected from the Bulletin of China Marine Disaster, <http://www.mnr.gov.cn/sj/sjfw/hy/gb/gg/zghyzhgb/>, accessed from 26 November 1990 to 26 April 2021. [48]). It is obvious that, after undertaking the relevant measures, the algal bloom decreased sharply, and the ecological environment was improved.

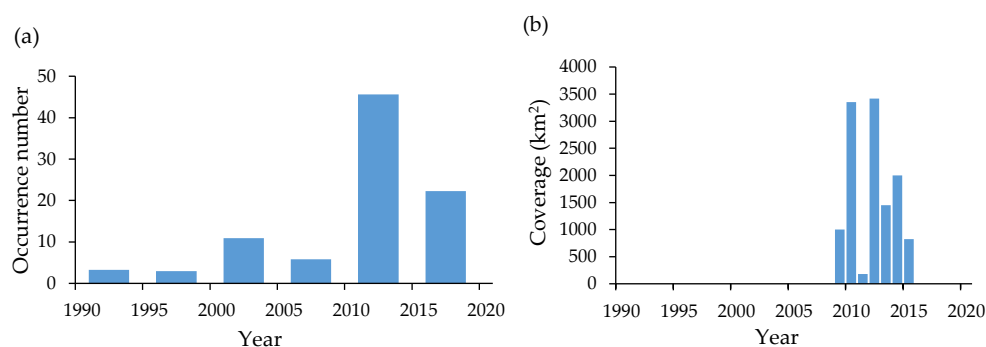


Figure 12. The occurrence number of red tide (a) and the *A. anophagefferens* coverage during the brown tide period (b) from 1990 to 2020.

Sufficient nutrients and low grazing pressure by zooplankton and scallops can accelerate the growth of small-celled phytoplankton [50], including *A. anophagefferens*. Previous studies have revealed the nutrient effects on brown tide blooms. As one of the dominant species in brown tide, *A. anophagefferens* has a considerable contribution to phytoplankton abundance [15,51] because it can outcompete other phytoplankton in the presence of elevated organic matter concentration [52]. The decreasing concentration of DIN, increasing human aquaculture activities, and suitability of summer temperatures for the growth of *A. anophagefferens* may be the primary causes of brown tide outbreaks [53]. Zhang et al. [54,55] analyzed the in situ data of the stations in Qinhuangdao and found that the DOP (dissolved organic phosphorus) can restrain *A. anophagefferens* growth, while DON showed great importance in causing brown tide.

With the continuous increase in the amount of national attention paid to the marine ecological environment, the concentration of nutrients, including nitrogen, in the seagoing rivers has significantly reduced. Considering the appropriate temperature, we can see that brown tide always blooms in summer, so the predicted time period is set from April to September. Therefore, we simulated the TN and transferred it into *A. anophagefferens* density to investigate the possibility of brown tide in recent years. We selected the TN concentration of July, August, and September in 2021 to convert into *A. anophagefferens* cell density (Figure 13). Although there exists a slightly higher area offshore compared to the open sea, it does not achieve the warning grade, indicating that this period experienced no danger of brown tide outbreak, and therefore the government just needed to conduct routine monitoring. The model results combine the transformation records, showing that water environment improvements reduced the degree of eutrophication to prevent brown tide from occurring in 2021.

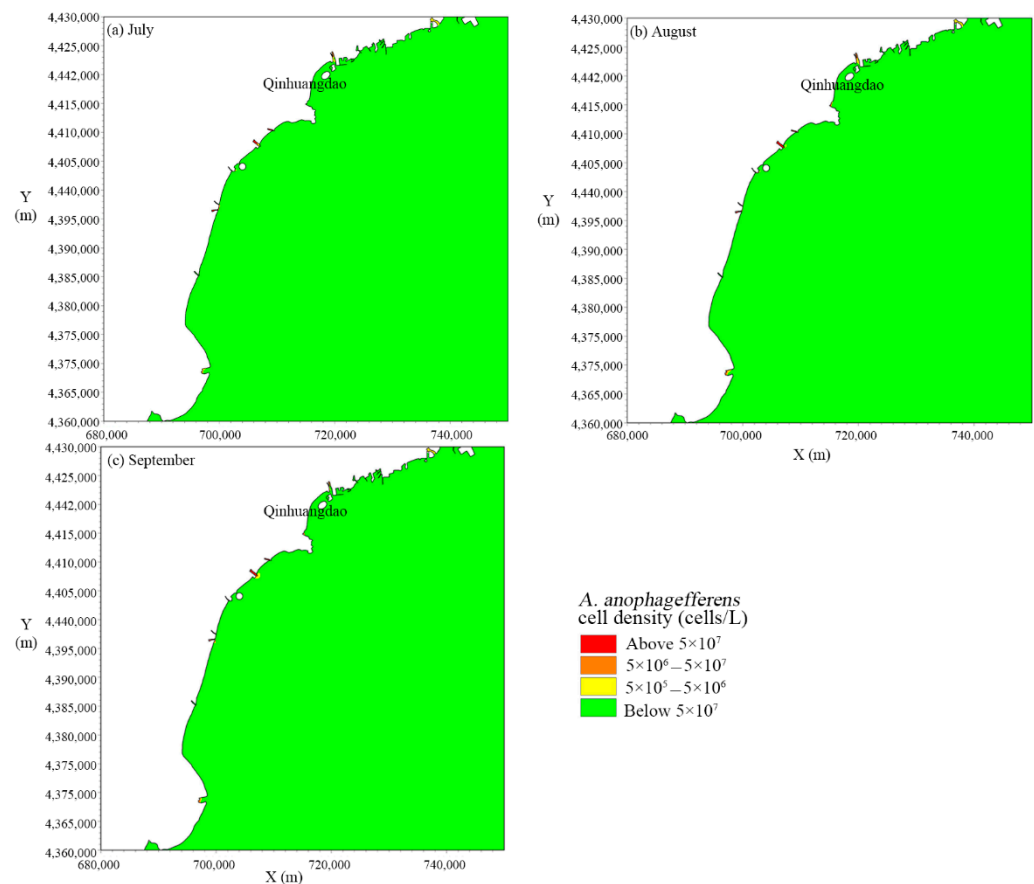


Figure 13. The distribution of *A. anophagefferens* cell distribution in July, August, and September 2021.

4.2. Comparison with Other Forewarning Systems

The aim of this study is mainly to provide a simple fast forewarning system for brown tide. A similar method was also studied by Guo et al. [56] in their forewarning system, with the indicator of Chl-a by establishing a coupled physical-chemistry-ecohydrodynamic module to simulate the growth, development, and decline of harmful algal bloom. The method for monitoring red tide and green tide has developed over many years, but brown tide has rarely been studied. Nowadays, satellite technology can enable the large-scale simultaneous monitoring of green tide [57]. During the bloom period in the Huanghai Sea, the satellite data of MERSI and HJ/CCD were applied to monitor green tide migration [58]. Allen et al. [59] took advantage of satellites combined with a model to monitor the chlorophyll and presented the medium resolution continental shelf (MRCS) to forecast red tide events. Sivapragasam et al. [60] established a numerical model using genetic programming and predicted the red tide event in Tolo Harbor in Hong Kong. Dippner et al. [61] presented a numerical model based on the HAMSOM model and the Lagrangian red-tide model. With the rapid development of computer technology and artificial intelligence, neural network models have gradually been applied to harmful algal bloom forecasting systems. Ma et al. [62] applied modified three-layer back propagation to forecast *Noctiluca scintillans*-induced red tide, and it performed well in reality. Velo-Suárez and Gutiérrez-Estrada [63] combined principal component analysis and a feed forward neural network to predict red tide bloom. However, the neural network model has a projecting defect of overdependence on the sample size, which may decrease the adaptability and tolerance. In recent years, harmful algal coupled monitoring and forecasting systems have drawn high levels of attention around the world [64]. Europe and some East Asian countries have distributed these systems, and the most important aim of these systems is to monitor for different kinds of algae [65].

For a fast forewarning system of brown tide in Qinhuangdao, a simple model, based on the 2D hydrodynamic and transport module to simulate the TN concentration, is adopted in the shallow coastal water where brown tides often occur in the summer season. A relationship between *A. anophagefferens* and TN obtained from field-measured data, combined with TN distribution from the transport module considering the decay, diffusion, and settling of TN, provided a fast forewarning system of brown tide in Qinhuangdao coastal water. This simple fast forewarning system of brown tide has been successfully used in Qinhuangdao and provided the local government with the ability to quickly conduct monitoring in the key areas of potential risk and take appropriate actions to mitigate brown tide. However, it has been proven by many previous studies that the vertical nutrient condition also plays a vital role in affecting harmful algal bloom [33]. In addition to nutrients, some other pressure variables, such as salinity, temperature, and the distribution of Chl-a, influence *A. anophagefferens* growth, migration, and spatiotemporal distribution [32]. Hence, a 3D-coupled model involving a hydrodynamic model, an ecological model, and a particle tracking model should be further established to simulate the real process of *A. anophagefferens*-induced brown tide, which is expected to be developed in following studies to improve the forewarning system.

5. Conclusions

In this study, the *A. anophagefferens*-induced brown tide in Qinhuangdao was investigated using a coupled hydrodynamic and particulate transport model based on MIKE 21. The hydrodynamic model was executed using a two-nested mesh system with different refinements and scales for the domains of the Bohai Sea and Qinhuangdao, respectively, and to predict the current to drive the transport model. This model considers the decay, diffusion, and settling of TN, and the model results are in good agreement with the measured tidal level, current, and TN, and thus the model is reliable. A relationship between *A. anophagefferens*, DON, and TN is obtained from field-measured data. This relationship and the numerically simulated TN distribution in Qinhuangdao can provide a fast forewarning system for brown tide. The fast routine assessment of brown tide by the present warning system provides robust guidance for the government to take action.

Due to the government having implemented various measures to protect the marine environment from harmful algal blooms, brown tide has been successfully mitigated in recent years. It is known that brown tide is not only affected by the *A. anophagefferens* cell density, but also by the vertical distribution of salinity and microorganisms; therefore, obtaining a better understanding of the mechanism of brown tide outbreak is of great importance. The present warning system only considers the single indicator of *A. anophagefferens* cell density, which has its limitations, and we will further improve it with a 3D model and neural networks and remote sensing technology.

Author Contributions: Conceptualization, C.K. and J.W.; methodology, C.K. and J.W.; software, J.W., J.F. and R.Q.; validation, J.W. and J.F.; investigation, L.O. and Q.Z. (Qingchun Zhang); data curation, L.O. and Q.Z. (Qingchun Zhang); writing—original draft preparation, J.W. and C.K.; writing—review and editing, C.K. and Q.Z. (Qingping Zou); supervision, C.K. and Q.Z. (Qingping Zou); funding acquisition, C.K. All authors have read and agreed to the published version of the manuscript.

Funding: This research was funded by the National Key Research and Development Project of China, under contract no. 2019YFC1407900, and the National Natural Science Foundation of China, under contract no. 41976159.

Institutional Review Board Statement: Not applicable.

Informed Consent Statement: Not applicable.

Data Availability Statement: Not applicable.

Acknowledgments: We are sincerely grateful to the Eighth Geological Brigade of the Hebei Geological Prospecting Bureau for supporting the fieldwork and measured data for the model validation. The last author has been supported by NERC, grant NE/V006088/1.

Conflicts of Interest: The authors declare no conflict of interest.

References

1. Yao, Z.; He, R.; Bao, X.; Wu, D.X.; Song, J. M2 tidal dynamics in Bohai and Yellow Seas: A hybrid data assimilative modeling study. *Ocean. Dyn.* **2012**, *62*, 753–769. [[CrossRef](#)]
2. Lee, H.S.; Lee, J.H.W. Continuous monitoring of short-term dissolved oxygen and algal dynamics. *Water Res.* **1995**, *29*, 2789–2796. [[CrossRef](#)]
3. Hallegraeff, G.M. A review of harmful algal blooms and their apparent global increase. *Phycologia* **1993**, *32*, 79–99. [[CrossRef](#)]
4. Anderson, D.M. Red tides. *Sci. Am.* **1994**, *271*, 62–68. [[CrossRef](#)] [[PubMed](#)]
5. Li, Y.; Huang, L.M.; Chen, J.F.; Zhou, M.J.; Tan, Y.T. Water quality and phytoplankton blooms in the Pearl River Estuary. In *The Environment in Asia Pacific Harbours*; Wolanski, E., Ed.; Springer: Berlin/Heidelberg, Germany, 2006; pp. 139–145.
6. Gobler, C.J.; Lonsdale, D.J.; Boyer, G.L. A review of the causes, effects, and potential management of harmful brown tide blooms caused by *Aureococcus anophagefferens* (Hargraves et Sieburth). *Estuaries* **2005**, *28*, 726–749. [[CrossRef](#)]
7. Olsen, P.S. Development and distribution of a brown-water algal bloom in Barnegat Bay, New Jersey with perspective on resources and other red tides in the region. *Coast. Estuar. Stud.* **1989**, *35*, 189–212.
8. Sieburth, J.M.; Johnson, P.W.; Hargraves, P.E. Ultrastructure and ecology of *Aureococcus anophagefferens* gen. et sp. Nov. (Chrysophyceae)—The dominant picoplankton during a bloom in Narragansett Bay, Rhode Island, summer 1985. *J. Phycol.* **1988**, *24*, 416–425. [[CrossRef](#)]
9. Pitcher, G.C.; Calder, D. Harmful algal blooms of the southern Benguela current: A review and appraisal of monitoring from 1989 to 1997. *South Afr. J. Mar. Sci.* **2000**, *22*, 255–271. [[CrossRef](#)]
10. Probyn, T.; Pitcher, G.; Pienaar, R.; Nuzzi, R. Brown tides and mariculture in Saldanha Bay, South Africa. *Mar. Pollut. Bull.* **2001**, *42*, 405–408. [[CrossRef](#)]
11. Coper, E.; Dennison, W.; Milligan, A.; Carpenter, E.; Lee, C.; Holzapfel, J.; Milanese, L. *An Examination of the Environmental Factors Important to Initiating and Sustaining “Brown Tide” Blooms*; Springer: Berlin/Heidelberg, Germany, 1989; pp. 317–340.
12. Zhang, Q.C.; Qiu, L.M.; Yu, R.C.; Kong, F.Z.; Wang, Y.F.; Yan, T.; Gobler, C.J.; Zhou, M.J. Emergence of brown tides caused by *Aureococcus anophagefferens* Hargraves et Sieburth in China. *Harmful Algae* **2012**, *19*, 117–124. [[CrossRef](#)]
13. Kong, F.Z.; Yu, R.C.; Zhang, Q.C.; Yan, T.; Zhou, M.J. Pigment characterization for the 2011 bloom in Qinhuangdao implicated “brown tide” events in China. *Chin. J. Oceanol. Limnol.* **2012**, *30*, 361–370. [[CrossRef](#)]
14. Qiao, L.; Chen, Y.H.; Mi, T.Z.; Zhen, Y.; Gao, Y.H.; Yu, Z.G. Quantitative PCR analysis of the spatiotemporal dynamics of *Aureococcus anophagefferens* and *Minutocellus polymorphus* and the relationship between brown tides and nutrients in the coastal waters of Qinhuangdao. *J. Appl. Phycol.* **2017**, *29*, 297–308. [[CrossRef](#)]
15. Zhen, Y.; Qiao, L.L.; Gu, B.; Mi, T.Z. Characteristics of eukaryotic microalgal community and its abiotic influencing factors during brown tide blooms near Qinhuangdao, China. *Harmful Algae* **2016**, *57*, 1–12. [[CrossRef](#)] [[PubMed](#)]
16. Yao, P.; Lei, L.; Zhao, B.; Wang, J.P.; Chen, L. Spatial-temporal variation of *Aureococcus anophagefferens* blooms in relation to environmental factors in the coastal waters of Qinhuangdao, China. *Harmful Algae* **2019**, *86*, 106–118. [[CrossRef](#)]
17. Yu, J.; Zhang, L.L.; Sun, Y.; Zhang, L.; Jiao, W.Q.; Dou, H.Q.; Guo, H.B.; Bao, Z.M. Diversity of nanoplankton during the brown tide in the Bohai Sea. *Period. Ocean. Univ. China* **2015**, *45*, 73–78.
18. Tang, Y.Z.; Ma, Z.P.; Hu, Z.H.; Deng, Y.Y.; Yang, A.A.; Lin, S.H.; Yi, L.; Chai, Z.Y.; Gobler, C.J. 3000 km and 1500-year presence of *Aureococcus anophagefferens* reveals indigenous origin of brown tides in China. *Mol. Ecol.* **2019**, *28*, 4065–4076. [[CrossRef](#)]
19. Wong, K.T.M.; Lee, J.H.W.; Hodgkiss, I.J. Forecasting of environmental risk maps of coastal algal blooms. *Harmful Algae* **2009**, *8*, 407–420. [[CrossRef](#)]
20. Ou, L.J.; Cai, Y.Y.; Jin, W.Y. Understanding the nitrogen uptake and assimilation of the Chinese strain of *Aureococcus anophagefferens* (Pelagophyceae). *Algal Res.* **2018**, *34*, 182–190. [[CrossRef](#)]
21. Bricelj, V.M.; Kuenster, S.H. Effects of the “brown tide” on the feeding physiology and growth of bay scallops and mussels. *Coast. Estuar. Stud.* **1989**, *35*, 491–509.
22. Reyhan, M. Effects of *Aureococcus anophagefferens* on Microzooplankton Grazing and Growth Rates in the Peconic Bays System, Long Island, New York. Ph.D. Thesis, Stony Brook University, Stony Brook, NY, USA, 1996.
23. Durbin, A.G.; Durbin, E.G. Effect of the “brown tide” on feeding, size and egg laying rate of adult female *Acartiatonsa*. In *Novel Phytoplankton Blooms*; Springer: Berlin/Heidelberg, Germany, 1989; pp. 625–646.
24. Duguay, L.; Monteleone, D. Abundance and distribution of zooplankton and ichthyoplankton in Great South Bay, New York during the brown tide outbreaks of 1985 and 1986. *Coast. Estuar. Stud.* **1989**, *35*, 599–623.
25. Caron, D.A.; Gobler, C.J.; Lonsdale, D.J.; Cerrato, R.M.; Schaffner, R.A.; Rose, J.M.; Buck, N.J.; Taylor, G.; Boissonneault, K.R.; Mehran, R. Microbial herbivory on the brown tide alga, *Aureococcus anophagefferens*: Results from natural ecosystems, mesocosms and laboratory experiments. *Harmful Algae* **2004**, *3*, 439–457. [[CrossRef](#)]

26. Smith, J.K.; Lonsdale, D.J.; Gobler, C.J.; Caron, D.A. Feeding behavior and development of *Acartia tonsa* nauplii on the brown tide alga *Aureococcus anophagefferens*. *J. Plankton Res.* **2008**, *30*, 937–950. [CrossRef]
27. Lonsdale, D.J.; Cosper, E.M.; Kim, W.S.; Doall, M.H.; Jonasdottir, S.H. Food web interactions in the plankton of Long Island bays, with preliminary observations on brown tide effects. *Mar. Ecol. Prog. Ser.* **1996**, *134*, 247–263. [CrossRef]
28. Anderson, D.M.; Glibert, P.M.; Burkholder, J.M. Harmful algal blooms and eutrophication: Nutrient sources, composition, and consequences. *Estuaries* **2002**, *25*, 704–726. [CrossRef]
29. Heisler, J.; Glibert, P.M.; Burkholder, J.M.; Anderson, D.M.; Cochlan, W.; Dennison, W.C.; Dortch, Q.; Gobler, C.J.; Heil, C.A.; Humphries, E.; et al. Eutrophication and harmful algal blooms: A scientific consensus. *Harmful Algae* **2008**, *8*, 3–13. [CrossRef]
30. O’Neil, J.M.; Davis, T.W.; Burford, M.A.; Golber, C.J. The rise of harmful cyanobacteria blooms: The potential roles of eutrophication and climate change. *Harmful Algae* **2012**, *9*, 123–133. [CrossRef]
31. Lee, J.H.W.; Qu, B. Hydrodynamic tracking of the massive spring 1998 red tide in Hong Kong. *J. Environ. Eng.* **2004**, *130*, 535–550. [CrossRef]
32. Zhang, Q.C.; Yu, R.C.; Zhao, J.Y.; Kong, F.Z.; Chen, Z.F.; Niu, Z.; Xiang, L. Distribution of *Aureococcus anophagefferens* in relation to environmental factors and implications for brown tide seed sources in Qinhuangdao coastal waters, China. *Harmful Algae* **2021**, *109*, 102105. [CrossRef]
33. Glibert, P.M.; Burford, M.A. Globally changing nutrient loads and harmful algal blooms: Recent advances, new paradigms, and continuing challenges. *Oceanography* **2017**, *30*, 58–69. [CrossRef]
34. Wong, K.T.M.; Lee, J.H.W.; Hodgkiss, I.J. A simple model for forecast of coastal algal blooms. *Estuar. Coast. Shelf Sci.* **2007**, *74*, 175–196. [CrossRef]
35. Hallegraeff, G.M. Ocean climate change, phytoplankton community responses, and harmful algal blooms: A formidable predictive challenge. *J. Phycol.* **2010**, *46*, 220–235. [CrossRef]
36. Gastrich, M.D.; Wazniak, C.E. A brown tide bloom index based on the potential harmful effects of the brown tide algae, *Aureococcus anophagefferens*. *Aquat. Ecosyst. Health Manag.* **2002**, *5*, 435–441. [CrossRef]
37. Zhang, Y.Q.; Yu, Z.M.; Song, X.X.; Gao, X.H.; Liu, Y. Study on removal of brown tide-*Aureococcus anophagefferens* by modified clay. *Acta Oceanol. Sin.* **2013**, *35*, 197–203.
38. Randhawa, V.; Thakkar, M.; Wei, L.P.; Shah, V. Applicability of Hydrogen Peroxide in Brown tide control-culture and microcosm studies. *PLoS ONE* **2012**, *7*, e47844. [CrossRef] [PubMed]
39. Xie, H.Y.; Wang, J.H.; Ma, Z.Y.; Fan, L.J. Review of harmful algal blooms hazard. *Mar. Environ. Sci.* **2019**, *38*, 482–488.
40. LaRoche, J.; Nuzzi, R.; Waters, R.; Wyman, K.; Falkowski, P.G.; Wallace, D.W.R. Brown tide blooms in long island’s coastal waters linked to interannual variability in groundwater flow. *Glob. Chang. Biol.* **1997**, *3*, 397–410. [CrossRef]
41. DHI Group. *Mike 21 & Mike 3 FLOW MODEL FM: Hydrodynamic and Transport Module Scientific Documentation*; DHI Group: Hørsholm, Denmark, 2021.
42. Dong, Z.; Kuang, C.; Gu, J.; Zou, Q.; Zhang, J.; Liu, H.; Zhu, L. Total Maximum Allocated Load of Chemical Oxygen Demand Near Qinhuangdao in Bohai Sea: Model and Field Observations. *Water* **2020**, *12*, 1141. [CrossRef]
43. Kuang, C.; Dong, Z.; Gu, J.; Su, T.-C.; Zhan, H.; Zhao, W. Quantifying the influence factors on water exchange capacity in a shallow coastal lagoon. *J. Hydro Environ. Res.* **2020**, *31*, 26–40. [CrossRef]
44. Willmott, C.J. On the validation of models. *Phys. Geogr.* **1981**, *2*, 184–194. [CrossRef]
45. DeYoe, H.R.; Stockwell, D.A.; Biologare, R.R.; Latasa, M.; Johnson, P.W.; Hargraves, P.E.; Suttle, C.A. Description and characterization of the algal species *Aureococcus anophagefferens* et sp. Nov. and referral of *Aureoombra* and *Aureococcus* to the Pelagophyceae. *J. Phycol.* **1997**, *33*, 1042–1048. [CrossRef]
46. Gobler, C.J.; Deonarine, S.; Leich-Bell, J.; Gastrich, M.D.; Anderson, Q.R.; Wilhelm, S.W. Ecology of phytoplankton communities dominated by *Aureococcus anophagefferens*: The role of viruses, nutrients, and microzooplankton grazing. *Harmful Algae* **2004**, *3*, 471–483. [CrossRef]
47. Mulholland, M.R.; Boneillo, G.E.; Bernhardt, P.W.; Elizabeth, C. Comparison of nutrient and microbial dynamics over a seasonal cycle in a mid-Atlantic coastal lagoon prone to *Aureococcus anophagefferens* (brown tide) blooms. *Estuaries Coasts* **2009**, *32*, 1176–1194. [CrossRef]
48. Ministry of Natural Resources of People’s Republic of China. Bulletin of China Marine Disaster. 1990–2020. Available online: <http://www.mnr.gov.cn/sj/sjfw/hy/gbgg/zghyzhgb/> (accessed on 26 April 2021).
49. Yu, Z.M.; Song, X.X.; Cao, X.H. Mitigation of harmful algal blooms using modified clays: Theory, mechanisms, and applications. *Harmful Algae* **2017**, *69*, 48–64. [CrossRef]
50. Qiao, L.; Yu, J.; Li, Y.; Guo, H.B.; Zhen, Y.; Zhang, L.L.; Mi, T.Z.; Zhang, F.C.; Bao, Z.M. Succession of the Nanoplankton Community during a brown tide in a scallop culture area in China. *Ocean Sci. J.* **2019**, *54*, 375–392. [CrossRef]
51. Gui, L.; Lu, X.X.; Dong, Y.L.; Cen, J.Y.; Cao, R.B.; Pan, L.; Lu, S.H.; Ou, L.J. Relationship between phytoplankton community succession and environmental parameters in Qinhuangdao coastal areas, China: A region with recurrent brown tide outbreaks. *Ecotoxicol. Environ. Saf.* **2018**, *159*, 85–93.
52. Gobler, C.J.; Berry, D.L.; Dyhrman, S.T.; Wilhelm, S.W.; Salamov, A.; Lobanov, A.V.; Zhang, Y.; Collier, J.L.; Wurch, L.L.; Kustka, A.B. Niche of harmful alga *Aureococcus anophagefferens* revealed through ecogenomics. *Proc. Natl. Acad. Sci. USA* **2011**, *108*, 4352–4357. [CrossRef]

53. Wetz, M.S.; Cira, E.K.; Boatwright, B.S.; Montagna, P.A.; Palmer, T.A.; Hayes, K.C. Exceptionally high organic nitrogen concentrations in a semi-arid South Texas estuary susceptible to brown tide blooms. *Estuar. Coast. Shelf Sci.* **2017**, *188*, 21–37. [[CrossRef](#)]
54. Zhang, J.L.; Wang, Q.Y.; Zhang, Y.F.; Zhang, W.L.; Li, L. Characteristics of seawater nutrients during the occurrence of brown tide in the coastal area of Qinhuangdao, China. *Chin. J. Appl. Ecol.* **2020**, *31*, 282–292.
55. Zhang, W.L.; Ma, X.; Zhang, Y.F.; Zhang, J.L.; Zhao, S.L.; Li, G.M. An analysis of red tide characteristics in Qinhuangdao coastal seawater. *Trans. Oceanol. Limnol.* **2020**, *5*, 48–55.
56. Guo, H.; Lin, F.A.; Liu, Y.J.; Xu, D.Y.; Lu, X.W. High-incidence HABs causative species in China Coastal Waters and the forewarning method based on the HABs Risk Index. *Mar. Environ. Sci.* **2014**, *33*, 94–98.
57. Liu, D.Y.; Keesing, J.K.; Xing, Q.; Shi, P. World's largest macroalgal bloom caused by expansion of seaweed aquaculture in China. *Mar. Pollut. Bull.* **2009**, *58*, 888–895. [[CrossRef](#)] [[PubMed](#)]
58. Zeng, T.; Liu, J.Q. The Application of Beijing-1 Micro Satellite Data to Algae Disaster Monitoring in the Sea of Qingdao. *Remote Sens. Inf.* **2009**, *3*, 34–37.
59. Allen, J.I.; Smyth, T.J.; Siddorn, J.R.; Holt, M. How well can we forecast high biomass algal bloom events in a eutrophic coastal sea. *Harmful Algae* **2008**, *8*, 70–76. [[CrossRef](#)]
60. Sivapragasam, C.; Muttill, N.; Muthukumar, S. Prediction of algal bloom using genetic programming. *Mar. Pollut. Bull.* **2010**, *60*, 1849–1855. [[CrossRef](#)] [[PubMed](#)]
61. Dipper, J.W.; Nguyen-Ngoc, L.; Doan-Nhu, H. A model for the prediction of harmful algae blooms in the Vietnamese upwelling area. *Harmful Algae* **2011**, *10*, 606–611.
62. Ma, Y.M.; Gao, J.Y.; Wang, Q.H. Forecast model for red tide on artificial neural network. *Mar. Forecast.* **2007**, *24*, 38–44.
63. Velo-Suárez, L.; Gutiérrez-Estrada, J.C. Artificial neural network approaches to one-step weekly prediction of *Dinophysis acuminata* blooms in Huelva (Western Andalucía, Spain). *Harmful Algae* **2007**, *6*, 361–371. [[CrossRef](#)]
64. Stauffer, B.A.; Bowers, H.A.; Buckley, E. Considerations in harmful algal bloom research and monitoring: Perspectives from a consensus-building workshop and technology testing. *Front. Mar. Sci.* **2019**, *6*, 399. [[CrossRef](#)]
65. Anderson, C.R.; Berdalet, E.; Kudela, R.M. Scaling up from regional case studies to a global harmful algal bloom observing system. *Front. Mar. Sci.* **2019**, *6*, 250. [[CrossRef](#)]